Indonesian Journal of Electrical Engineering and Computer Science
Vol. 1, No. 2, February 2016, pp. 238 ~ 248
DOI: 10.11591/ijeecs.v1.i2.pp238-248

High Penetration PV in Distribution Networks, Design and Control

Ashkan Mohammadi, Saman Hosseini
Eslamabad-E-Gharb Branch, Islamic Azad University, Eslamabad-E-Gharb, Iran
Corresponding author, e-mail: Ashkan.m@live.com

Abstract

Global warming is a direct consequence of consumption of fossil fuels which emit greenhouse gasses as they produce energy. Solar energy is the most available energy throughout the world in which regardless of capital investment is free and most importantly clean and emission free and could be a solution for global warming along with other renewable sources of energy. But as photovoltaic energy is becoming widespread and penetration level of photovoltaic power plants increase, several issues rise in distribution networks. In this paper, a high penetration photovoltaic power plant is designed and issues associated with it are thoroughly discussed. Voltage rise and cloud passage effect are amongst the most challenging issues in design and implementation of a high penetration photovoltaic power plant in distribution networks. Transient effects of cloud passage could lead to unacceptably low voltage in Point of Common Coupling and maximum penetration level must be set according to these issues. An efficient Maximum Power Point Tracking (MPPT) and a DC link voltage control scheme are also presented. Simulations have been done in Matlab/Simulink environment.

1. Introduction

The continuous increase in the level of greenhouse gas emissions and the climb in fuel prices are the main driving forces behind efforts to utilize various sources of renewable energy [1, 2]. In recent years there has been a growing attention towards use of solar energy. The main advantages of photovoltaic (PV) systems employed for harnessing solar energy are lack of greenhouse gas emission, low maintenance costs, fewer limitations with regard to site of installation and absence of mechanical noise arising from moving parts.

The market of PV energy has been in an increasing trend with the annual growth rate of 25-35% over the last ten years and 156% and 85% annual growth rate in US only in 2012 and 2013 respectively. As the use of solar PV continues to expand, concern about its potential impact on the stability and operation of the grid grow too. Utilities and power system operators are preparing for changes to integrate and manage more of this renewable electricity source in their systems.

The penetration level is defined as the ratio of nameplate PV power rating to the maximum load seen on the distribution feeder. The voltage rise issue has been reported as one of the concerns under high penetration of renewable Distributed Generations (DG) [3]. The reverse power flow caused by large amounts of DG may cause voltage rise to which distribution network operators control cannot effectively respond since the traditional grid has been planned to deliver power to the load at satisfactory voltage range [4].

Reference [5, 6] concentrated on distributed generators interfaced to utilities through inverters, and larger-scale system impacts and rotating distributed generation (DG), but still with several results on inverter-based DG. The first study [5] concluded that for DG penetration levels of 40%, such that the system is heavily dependent on DGs to satisfy loads, voltage regulation can become a serious problem. The sudden loss of DGs, particularly as a result of false tripping during voltage or frequency events, can lead to unacceptably low voltages in portions of the system. The same may occur in high penetration PV systems in which the microgrid is heavily dependent on photovoltaic energy to provide the local load with active power. In this situation, transient effect of cloud passage could lead to low voltage issue since the response time of On-Load Tap Changing (OLTC) transformers have few to several seconds delay.

Received September 22, 2015; Revised November 29, 2015; Accepted December 18, 2015

Referemce [7] examined cloud transient effects if the PV were deployed as a central-station plant, and it was found that the maximum tolerable system level penetration level of PV was approximately 5%, the limit being imposed by the transient following capabilities (ramp rates) of the conventional generators. Reference [8] focus on the operating experience of the Southern California Edison central-station PV plant at Hesperia, CA, which reported no such problems, but suggests that this plant had a very ‘‘stiff’’ connection to the grid and represented a very low PV penetration level at its point of interconnection.

Reference [9] dealt with voltage regulation issues on the Public Service Company of Oklahoma system during the passage of clouds over an area with high PV penetration levels, if the PV were distributed over a wide area. At penetration levels of 15%, cloud transients were found to cause significant but solvable power swing issues at the system level, and thus 15% was deemed to be the maximum system level penetration level.

In this paper a high penetration PV power plant connected to the distribution network feeder will be designed and controlled. The organization of the rest of this paper is as follows: in section 2 high penetration levels of PV energy and its consequences will be discussed. In section 3 equipment models used in this research are presented. The design procedure and control method will be discussed in section 4. In section 5 the simulation results and discussions are presented and finally conclusions close the paper.

2. Impact of High Penetration PV on Distribution Network

As the penetration level of distributed energy resources increase, several issues rise in distribution networks with regard to control, operation, protection and power quality. Voltage rise, cloud transient effect and higher Total Harmonic Distortion (THD) are the most important issues associated with high penetration PV power plants.

ANSI C84.1 specifies utilization voltage, which refers to the voltage at the point of use where the outlet equipment is plugged in. Furthermore, two ranges are defined, Range A is recommended for normal operating conditions, while Range B corresponds to unusual conditions, so the occurrence has to be limited in time duration and frequency. Recommended service and utilization voltage limits according to ANSI C84.1 are shown in Table 1. Utilities are generally concerned with maintaining the service voltage within acceptable limits; the utilization voltage then follows automatically, provided that the house wiring is done according to building codes.

Table 1. ANSI C84.1 voltage range

	Service		Utilization	
	Min	Max	Min	Max
Range A (normal)	-5%	+5%	-8.3%	+4.2%
Range B (emergency)	-8.3%	+5.8%	-11.7%	+5.8%

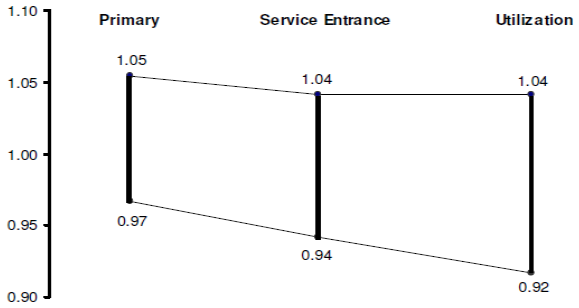

Figure 1. Voltage limits in distribution networks according to [10]

Figure 1 shows an example of voltage limits for primary circuit, service entrance, and utilization based on one utility's guidelines [10, 11]. It reflects the adjustment for assumptions about additional voltage drop in the secondary circuit and allows for the necessary margin. In this study, the primary voltage and service entrance voltage limits shown in Figure 1 were used as target limits.

3. PV and Inverter Model

3.1. PV Model

Figure 2 shows the equivalent circuit of a solar panel. A solar panel is composed of several photovoltaic cells that have series or parallel or series-parallel external connections. Equation (1) shows V-I characteristic of a solar panel [12].

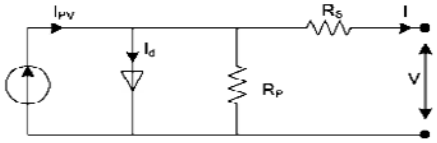

Figure 2. Equivalent circuit of Solar Panel

$$I = I_{pv} - I_o[\exp(\frac{V + R_S I}{aV_t}) - 1] - \frac{V + R_S I}{R_p} \quad (1)$$

Where I_{pv} is the photovoltaic current, I_o is saturated reverse current, 'a' is the ideal diode constant, $V_t = N_S KT/q$ is the thermal voltage, N_s is the number of series cells, q is the electron charge, K is the Boltzmann constant, T is the temperature of p-n junction, R_S and R_p are series and parallel equivalent resistance of the solar panels. I_{pv} has a linear relation with light intensity and also varies with temperature variations. I_o is dependent on temperature variations. Values of I_{pv} and I_o are calculated according to the following equations:

$$I_{pv} = (I_{pv,n} + K_I \Delta T)\frac{G}{G_n} \quad (2)$$

$$I_o = \frac{I_{sc,n} + K_I \Delta T}{\exp(V_{oc,n} + K_V \Delta T)/aV_t - 1} \quad (3)$$

In which $I_{pv,n}$, $I_{sc,n}$ and $V_{oc,n}$ are photovoltaic current, short circuit current and open circuit voltage in standard conditions (T_n = 25 C and G_n= 1000 W / m ^ 2) respectively. K_I is the coefficient of short-circuit current to temperature, $\Delta T = T - T_n$ is the temperature deviation from standard temperature, G is the light intensity and K_V is the ratio coefficient of open circuit voltage to temperature.

Open circuit voltage, short circuit current and voltage – current corresponding to the maximum power are three important points of I-V characteristic of Solar Panel. These points are changed by variations of atmospheric conditions. Using Equation (4) and (5) which are derived from PV model equations, short circuit current and open circuit voltage can be calculated in different atmospheric conditions.

$$I_{sc} = (I_{sc,n} + K_I \Delta T)\frac{G}{G_n} \quad (4)$$

$$V_{oc} = V_{oc,n} + K_V \Delta T \quad (5)$$

3.2. Hysteresis Current Control (HCC) of Power Electronic Unit

Hysteresis control presents an alternative method for producing a sinusoidal ac current waveform from a dc voltage source. With this method, the controller maintains an output current that stays within a given tolerance of the reference waveform. The tolerance that the output stays within is called the “hysteresis band”. Unlike the PWM switching technique, the method of hysteresis control depends on feedback from the output current to control the inverter system. The closed-loop control method enables the inverter with hysteresis control to adapt instantly to changes in the output loading.

The concept of hysteresis control can be applied to a wide range of inverter configurations and topologies. Both single-phase and three-phase inverters can be controlled by the hysteresis method as well. A common topology for single-phase inverters is the H-bridge because it offers more controllability than the half-bridge type. It allows the use of three output states instead of two and requires half of the dc bus voltage to produce the same peak output voltage [13]. Figure 3 illustrates the fundamental concept of operation for the hysteresis-controlled inverter.

The reference current,I_{ref}, represents the desired waveform for the output load current. The top and bottom hysteresis limits form the hysteresis band, which corresponds to the tolerance limit of the inverter controller.

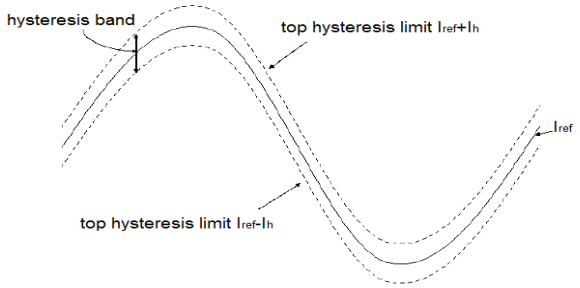

Figure 3. Concept of hysteresis band and hysteresis controller

The two-level inverter controller will apply the positive or negative dc bus voltage to the load in order to keep the output current within the hysteresis band. For example, when the output current rises above the top hysteresis limit, the inverter controller will respond by switching the transistors to apply the negative dc bus voltage to the load and effectively reduce the value of the output current to bring it below the top hysteresis limit. The inverter controller will keep the negative dc bus voltage across the load until the output current reaches the bottom hysteresis limit. After the output current drops below the bottom limit, the inverter controller will send the appropriate gating signals to the transistors to switch them to apply the positive dc bus voltage across the load. This will bring the output current back up above the bottom hysteresis limit and within the allowable tolerance band around the reference waveform. The controller will continuously repeat this cycle to maintain the output load current within the hysteresis band.

Unlike other high-fidelity inverter control strategies, the hysteresis controller will operate at a variable switching frequency that is spread across the spectrum. The instantaneous switching frequency $f_s$at any point on the current waveform can be predicted by [14]:

$$f_s = \frac{(V_{DC} - |I_{ref}|)|I_{ref}|}{LhV_{DC}} \quad (6)$$

Where V_{DC} is the dc bus voltage, I_{ref} is the instantaneous voltage of reference current signal, L is the load inductance, and h is the width of the hysteresis band. As reflected in Equation (6), the hysteresis inverter will switch faster at points in the cycle where the reference current reaches its maximum and minimum values and switch much slower when I_{ref} is close to zero in magnitude. A larger load inductance will allow the inverter to switch at a lower frequency to maintain the current within the same hysteresis band. Since f_s will diverge to infinity if L is equal

to zero, there must be some inductance present in the load for the hysteresis-controlled inverter to work. The switching frequency is also inversely proportional to$h$. The inverter will switch at higher rates overall to achieve a higher fidelity output current within a smaller hysteresis band.

Figure 4 shows a HCC for a single phase VSI. Assume the VSI terminal voltage V connects to a sinusoidal voltage source e through an equivalent inductance L and resistance R. If we want to control output current i to track a certain reference current i*, according to Figure 4(a) we have instantaneous value equation as:

$$L\frac{di}{dt} + Ri = V - e \tag{7}$$

When the SOFC output current is equal to reference current i*, the corresponding equation will be:

$$L\frac{di^*}{dt} + Ri^* = V^* - e \tag{8}$$

Where V* is the reference VSI terminal voltage corresponding to i*. If we define current tracking error Δi=i-i*, it is clear that when R=0, we have:

$$L\frac{d\Delta i}{dt} = V - V^* \tag{9}$$

Where VSI terminal voltage V is:

$$V = \begin{cases} \frac{E}{2} & (s = 1) \\ -\frac{E}{2} & (s = 0) \end{cases} \tag{10}$$

Where E is the VSI dc voltage and s the solid-state switch status. When Δi is greater than zero and beyond the tolerance, s is controlled to be at lower level s=0 and therefore (V-V*)<0 (note the dc voltage should be big enough for effective current tracking) which makes Δi to reduce. In the same way if Δi<0 and beyond the tolerance, s is controlled to be at higher-level s=1 and therefore (V-V*)>0 which makes Δi to increase. The corresponding hysteresis current control block diagram is shown in Figure 4.

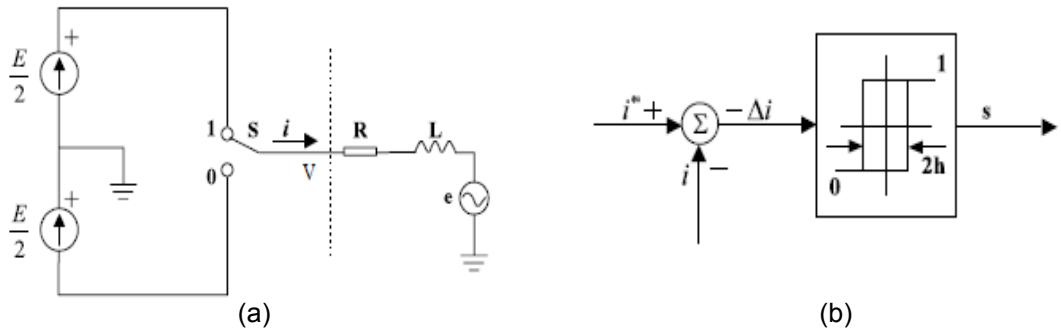

(a) (b)

Figure 4. Single phase VSI and HCC

4. Control and Coordination Scheme

4.1. MPPT Algorithm

In [15] a simple hybrid method has been proposed for MPPT of solar arrays. This algorithm consists of two stages; the first one is to estimate the voltage of maximum power point (V_{MPP}) and the second is to track the exact maximum power point using the classic Perturbation and Observation (P&O) with a small amplitude and frequency of perturbations. In the first stage, V_{MPP} is calculated using Equation (5) which is a linear equation in terms of temperature. Using that method, there is no need to disconnect the solar panel in order to measure the open circuit

voltage. This method has lower power oscillations and higher efficiency also better tracking performance in rapid changes of light intensity and temperature.

In this section, an improved hybrid method for MPPT will be proposed. In this method instead of calculating V_{MPP}, the current of the maximum power point (I_{MPP}) is calculated. This leads to an improved efficiency and higher accuracy [16]. The overall algorithm of the improved hybrid MPPT method has been shown in Figure 5. The relation between output current and voltage of PV array has been shown in Equation (1). In this equation, three parameters of 'a', R_S and R_P are not given by the manufacturer. In datasheet of a given PV array there is usually three pints of V-I characteristics given by the manufacturer which are short circuit current, open circuit voltage and voltage and current of maximum power point in standard atmospheric condition of 1000 w/m^2 and 25°C. By substituting these three points in Equation (12) and solving set of Equation of (1) three parameters of 'a', R_S and R_P will be determined.

$$\begin{cases} I_{SC,n} = I_{PV,n} - I_{O,n}\left(\exp(\frac{I_{SC,n}R_S}{aV_{T,n}}) - 1\right) - \frac{I_{SC,n}R_S}{R_P} \\ 0 = I_{PV,n} - I_{O,n}\left(\exp(\frac{V_{OC,n}}{aV_{T,n}}) - 1\right) - \frac{V_{OC,n}}{R_P} \qquad \rightarrow a, R_S, R_P \\ I_{MPP,n} = I_{PV,n} - I_{O,n}\left(\exp(\frac{I_{MPP,n}R_S}{aV_{T,n}}) - 1\right) - \frac{I_{MPP,n}R_S}{R_P} \end{cases} \tag{11}$$

To estimate the maximum power point current in each atmospheric condition we need the short circuit current in that atmospheric condition. In previous methods, the measurement was done by disconnecting the load actually short circuiting the terminals of the panel. In this proposed MPPT method, the short circuit current will be calculated using mathematical equations and measurement of output voltage and current of PV. The instantaneous values of voltage, current and temperature of the solar panel are measured and I_{PV} in which is the only variable dependent on light intensity in and also to temperature will be calculated using Equation (12). In this equation, V_T and I_O which are temperature dependent are updated using $V_t = N_S KT / q$ and Equation (3).

$$I_{PV} = I + I_O\left(\exp(\frac{V + IR_S}{aV_T}) - 1\right) + \frac{V + IR_S}{R_P} \tag{12}$$

Knowing I_{PV}, the nonlinear Equation (12) will be solved iteratively to calculate I_{SC}. This iterative equation will be repeated m times and in each iteration, I_{SC} of the previous iteration will be substituted (Equation (13)). After m iteration I_{SC} no longer varies which is indicative of convergence of the short circuit current. 'm' is a small integer because I_{PV}, which is the first estimation of I_{SC}, is very close to it. In other words in a few iterations I_{SC} will be found with an acceptable approximation.

$$\begin{aligned} & I_{SC,1} = I_{PV} \\ & I_{SC,m+1} = I_{PV} - I_O\left(\exp(\frac{I_{SC,m}R_S}{aV_T}) - 1\right) - \frac{I_{SC,m}R_S}{R_P} \\ & m = 1, 2, \ldots m \quad , \quad I_{SC} = I_{SC,m+1} \end{aligned} \tag{13}$$

In the proposed method, the fine tuning loop is used to correct the calculation of the I_{SC} to compensate the effect of the measurement error and possible model mismatch of solar panel. In this method, In case of small variations of temperature and I_{PV}, the fine tuning loop regulates output power. Since I_{PV} varies with radiation intensity, it can be inferred that the fine tuning loop will be run when atmospheric conditions are approximately constant. Consequently because in rapid changes of atmospheric conditions the fine tuning loop is not run, the amplitude of the perturbations of the P&O algorithm does not need to be great which will in turn will result in small variations of power in steady state conditions around the optimal value.

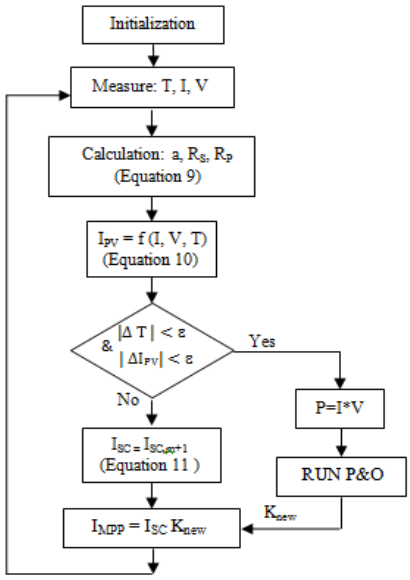

Figure 5. The flowchart of the proposed MPPT method

4.2. DC Link Voltage Control

The overall algorithm of the DC link voltage control strategy has been shown in Figure 6. This algorithm consists of two main modes. One mode is when the PV generates power ($P_{PV}>P_{min}$). This power will be delivered to the network through the Hysteresis Controlled Inverter. The other mode is when the power generated by the PV is less than the threshold P_{min}. In both modes, V_{DC} must be greater than V_{min} in order to have a satisfactory operation of the inverter.

In the first mode, the generated power of the PV is delivered to the DC link through a boost converter. When V_{DC} is less than the threshold (V_{DC-min}), according to the control strategy the power of the PV is fed to the DC link to maintain in acceptable range. In this situation, the power delivered to P_g is zero, in other words the power of the PV is solely dedicated to charge the capacitor of the DC link. In a situation where V_{DC} is greater than V_{DC-min} a portion of the P_{PV} is used to charge the capacitor and the rest will be delivered to the grid through the inverter. When V_{DC} reaches maximum allowable voltage V_{DC-max}, the power of the PV is all fed to the grid. When V_{DC} is between V_{DC-min} and V_{DC-max} there is a linear relationship between the power used to charge the capacitor and the V_{DC-max}-V_{DC}.

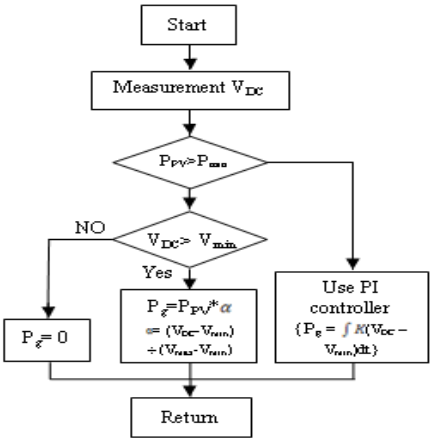

Figure 6. The overal algorithm of the DC link voltage control

4.3. Safe Operation Zone (SOZ)

In this paper, we assume that the nominal voltage of the distribution network is the voltage which is measured in zero penetration level. Any higher voltage is overvoltage and any lower voltage is undervoltage. The microgrid in this research comprises of a PV power plant with boost converter and hysteresiscurrent controlled inverter and a DC link and also a constant load. This microgrid is connected to the grid via an On-load Tap Changing transformer (OLTC).

The traditional distribution system has been designed as a unidirectional power flow network. As more and more distributed renewable sources are connected to the grid, the original unidirectional network will be changed toward the bidirectional network in the future. This change brings utility operation issues such as the voltage rise problem caused by the reverse power flow from the distributed renewable energy generation. Figure 7 illustrates the one line diagram of the simplified distribution network. There is a distributed generator connected to the load side. The generator voltage V_G can be approximately expressed in:

$$V_G \approx V_2 + R(P_G - P_L) + X(Q_G - Q_L) \quad (14)$$

Where V_2 is the substation secondary bus voltage, X is the feeder line reactance and R is feeder line resistance. P_G and Q_G are the real and reactive power provided by the generator, respectively. P_L and Q_L are the real and reactive power consumed by the load.

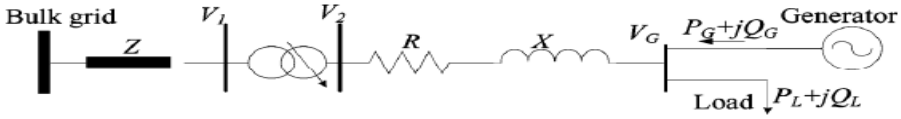

Figure 7. One line diagram of a typical grid connected DG

Equation (14) shows that the generator voltage may be higher than the upper-limit if the network X/R ratio is relatively low and there is a significant reverse power flow. One solution is that the generators can absorb a relatively large reactive power to compensate the reverse power flow. The alternative solution is that the substation secondary voltage can be correspondingly controlled or the real power injection to the grid can be decreased.

Currently, standards such as IEEE 1547 and UL1741 state that the PV inverter "shall not actively regulate the voltage at the PCC." Therefore, PV systems are designed to operate at unity power factor (i.e., provide only active power) because this condition will produce the most real power and energy. This limitation is a matter of agreement instead of a technical one; many inverters have the capability of providing reactive power to the grid in addition to the active power generated by their PV cells. The amount of reactive power (*Q*) available from the inverter depends on its ratings (*S*) and the active power (*Ppv*) supplied by the PV array. Consequently, the inverter can use its entire rating to supply *Q* if *Ppv* equals zero (there is no sun), and at the other extreme, it has no *Q* capability if *Ppv* equals *S*. Some *Q* capability can always be retained by over-sizing the inverter. In addition to the continuous reactive power support, inverters can operate very fast (milliseconds to microseconds with high switching frequency inverters) compared to capacitors, which can cause switching transients.

In this paper, a safe operation zone (SOZ) will be proposed according to the load impedance of grid and transformers and a safe penetration level will be derived. SOZ is the zone in which according to nominal irradiance and temperature conditions of a certain geographic site, load level and grid characteristics, the devised penetration level would not cause over voltages above the ANSI standards.

5. Simulation and Discussions

5.1. System Description

The model of PV array has been presented in section 3. The PV array is connected to the inverter via a boost converter. A capacitor is connected to the output of the boost converter to provide transient energy storage capability. A hysteresis controlled inverter connects DC link to the PCC via a RL filter. Distribution network lines are simulated as RL impedances which

connect grid voltage source to the OLTC. A schematic of the overall power systems is shown in Figure 8.

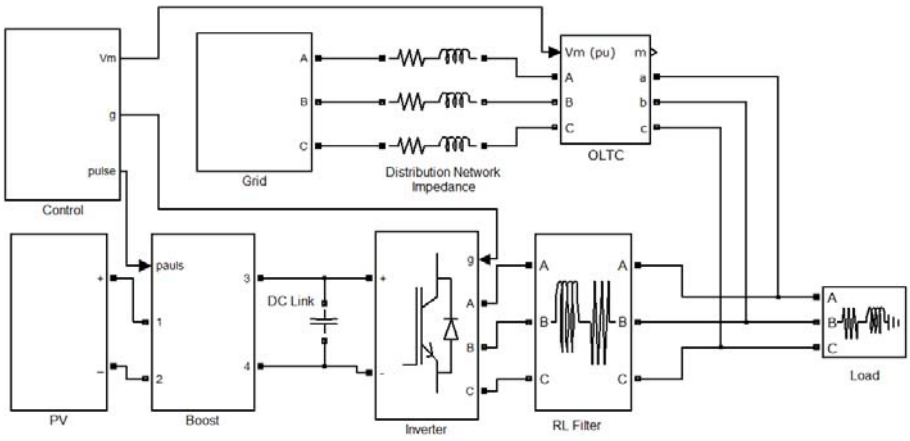

Figure 8. The block diagram of the grid connected photovoltaic power plant with high penetration level

5.2. Simulation Results

Table 2 and 3 show the PV and load power, voltage of the grid at the PCC and the corresponding penetration level for three different loadings. As can be seen, as the penetration level increases, the voltage of common coupling also raises. The maximum acceptable voltage in this microgrid is 395v and consequently the maximum penetration level for 100kw loading in this microgrid is 28%. For 70kw loading, maximum penetration levels is 38%.

Table 2. Different penetration levels of PV for 100kw nominal local load

PV power	Load power	voltage	PL
0	100.05	380.1	0
10.5	102.8	385.3	10.21401
22.8	106	391.3	21.50943
35.25	109.2	397.2	32.28022
41.5	110.8	400.13	37.45487
47.7	112.4	403	42.43772
58.6	115.5	407.6	50.73593

Table 3. Different penetration levels of PV for 100kw nominal local load

PV power	Load power	voltage	PL
0	70.04	380.39	0
10.5	72.15	385.8	14.55301
19.72	73.95	390.5	26.66667
29.05	75.6	395.15	38.42593
38.4	77.4	399.75	49.6124
47.75	79.1	404.19	60.36662

The amount of penetration level could be more if the OLTC is set accordingly. For example if desired maximum penetration level is 60% the output voltage of OLTC should be set so that in normal operation of the microgrid (nominal load and PV penetration) the voltage of PCC remains in allowed range. Since the amount of power generated by PV is a function of solar irradiance and it is not constant throughout the day, the output voltage of OLTC should be designed for maximum expected solar irradiance (maximum expected penetration level). In this situation, the limiting factor would not be the overvoltage problem issues like cloud passage, load change and THD rate could limit the penetration level.

Cloud passage which imposes a shadow on PV arrays suddenly decreases the amount of irradiance on PV array. Consequently The amount of power generated by PV power plant decreases. The effect of this decrease in generated power is power deficiency which needs to be compensated by additional grid power. Increase of grid power will also increase the grid current and will result in voltage drop in PCC due to distribution network impedance. The amount of voltage drop depends on the distribution network impedance, loading, penetration level and characteristics of the cloud.

Figure 9 and Figure 10 show the simulation of a cloud passage over the microgrid and its effects on voltage profile and power balance of microgrid and distribution network. The shadow of the cloud has been simulated as a 25% decrease in solar irradiance over the period of 1s. As can be seen, the voltage of PCC suddenly decreases as the power injected by PV decreases due to decrease in solar irradiance. The shortcoming of power needs to be compensated by grid power and as the current flows from the grid to PCC, it will cause more voltage drop on impedance of the grid. In this simulation it is assumed that the nominal voltage of PCC has been set according to 60% of penetration level by means of OLTC. In other words, in 60% of penetration level, and with 100kw of loading, the voltage of PCC has been set to 380v using OLTC.

The power of grid, load and PV is shown in Figure 9. As can be seen, the shortcoming power is provided by grid immediately. In photovoltaic power plants with higher power rates, the response time of grid's synchronous generators could also put a constraint on the penetration level as the shortcoming power could not immediately be provided by grid. This limit is imposed by the transient following capabilities (ramp rates) of the conventional generators [70]. As can be seen in fig (10), in 25% decrease in solar irradiance, the voltage of PCC drops to 370.5v which is 97.5% of nominal voltage which is in acceptable range according to utility standards.

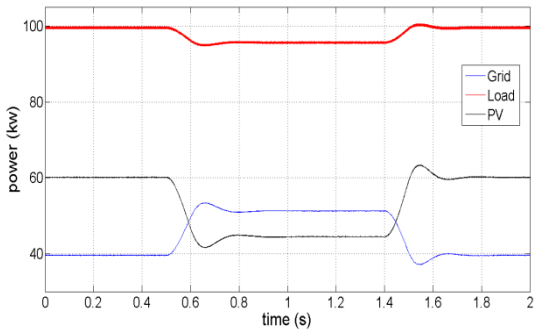

Figure 9. Power balance of microgrid as imposed by cloud passage with 25% solar irradiance decrease

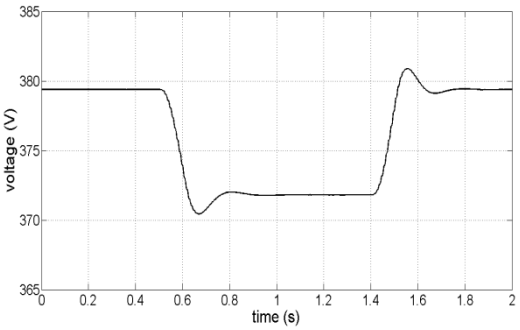

Figure 10. Voltage of PCC in 25% solar irradiance decrease

Figure 11 shows the power balance of microgrid in 50% decrease in solar irradiance. As can be seen, from 0.5s to 1.5s solar irradiance decreases 50% and photovoltaic power provided by PV also decreases. The corresponding PCC voltage is shown in Figure 12. By increase of grid power, the voltage drop also increases and will result in voltage sag in PCC. The voltage sag accounts for 5.2% of nominal voltage.

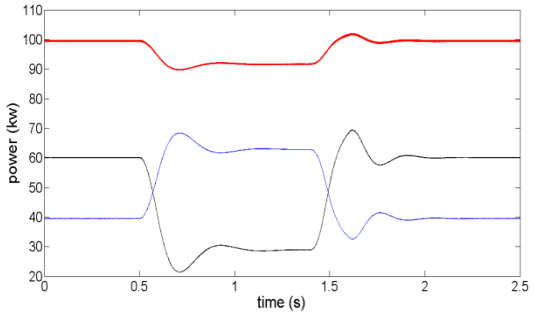

Figure 11. Power balance of microgrid as imposed by cloud passage with 50% solar irradiance decrease

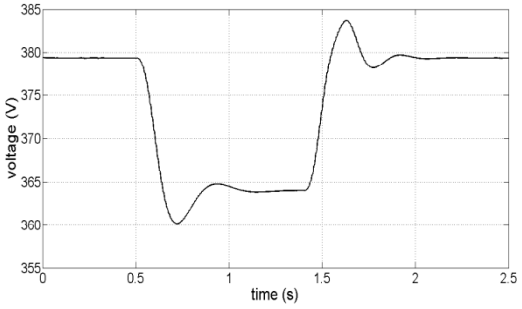

Figure 12. Voltage of PCC in 50% solar irradiance decrease

6. Conclusion

In this paper, a high penetration photovoltaic power plant was designed and issues associated with it were thoroughly discussed. Voltage rise and cloud passage effect are amongst the most challenging issues in design and implementation of a high penetration photovoltaic power plant in distribution networks. Transient effects of cloud passage could lead to unacceptably low voltage in Point of Common Coupling and maximum penetration level must be set according to these issues. An efficient Maximum Power Point Tracking (MPPT) and a DC link voltage control scheme were also presented. Simulations have been done in Matlab/Simulink environment. A safe operation zone for PV power plant was determined in which according to maximum output power of the PV power plant in specific geographical site the maximum allowable penetration level was found.

References

[1] Wu TF, Chang CH, Liu ZR, Yu TH. *Single-stage converters for photovoltaic powered lighting systems with MPPT and charging features*. In Proc. IEEE APEC. 1998: 1149-1155.
[2] De Broe AM, Drouilhet S, Gevorgian V. A peak power tracker for small wind turbines in battery charging applications. *IEEE Transactions on Energy Conversion*. 1999; 14(4): 1630-1635.
[3] CL Masters. Voltage rise: The big issue when connecting embedded generation to long 11 kV overhead lines. *Inst. Elect. Eng. Power Eng. J.* 2002: 16(1): 5–12.
[4] P Carvalho, P Correia, L Ferreira. Distributed reactive power generation control for voltage risemitigation in distribution networks. *IEEE Trans. Power Syst.*, 2008; 23(2): 766–772.
[5] NREL report NREL/SR-560-34635. DG power quality, protection, and reliability case studies report. General Electric Corporate R&D. 2003.
[6] NREL report NREL/SR-560-34715. Report on distributed generation penetration study. 2003.
[7] Chalmers S, Hitt M, Underhill J, Anderson P, Vogt P, Ingersoll R. The effect of photovoltaic power generation on utility operation. *IEEE Transactions on Power Apparatus and Systems.* 1985; 104(3): 524-530.
[8] Patapoff N, Mattijetz D. Utility interconnection experience with an operating central station MW-Sized photovoltaic plant. *IEEE Transactions on Power Systems and Apparatus.* 1985; 104(8): 2020-2024.
[9] Jewell W, Ramakumar R, Hill S. A study of dispersed PV generation on the PSO system. *IEEE Transactions on Energy Conversion.* 1988; 3(3): 473-478.
[10] H Lee Willis. Power Distribution Planning Reference Book. CRC Press. 2004.
[11] Tom Short. Electric Power Distribution Handbook. CRC Press. 2003.
[12] MG Villalva, JR Gazoli, ER Filho. Comprehensive approach to modeling and simulation of photovoltaic arrays. I*EEE Trans. Power Electron*. 2009; 24(5): 1198-1208.
[13] Ned Mohan Tore M Undeland, William P Robbins. Power Electronics. 3rd Edition. Hoboken, New Jersey: John Wiley and Sons, Inc. 2003: 40-42, 204-239
[14] Allie Auld, Fabian Mueller, Keyue Ma Smedley, Scott Samuelsen, Jack Brouwer. Applications of one-cycle control to improve the interconnection of a solid oxide fuel cell and electric power system with a dynamic load. *Journal of Power Sources.* 2008; 179: 155-163.
[15] MH Moradi, AR Reisi. A hybrid maximum power point tracking method for photovoltaic systems. *Solar Energy*. 2011; 85: 2965-2976.
[16] T Noguchi, S Togashi, R Nakamoto. Short-current pulse-based maximum-power-point tracking method for multiple photovoltaic-and-converter module system. *IEEE Trans Ind Electron*. 2002; 49(1): 217-223.